Excited-State Dynamics of a D−π−A Type Sulfonium-Based Alkoxystilbene Photoacid Generator

ARTICLE *in* CHEMISTRY OF MATERIALS · MARCH 2015

Impact Factor: 8.35 · DOI: 10.1021/cm504474g

8 AUTHORS, INCLUDING:

Hélène Chaumeil
Université de Haute-Alsace
55 PUBLICATIONS **414** CITATIONS
SEE PROFILE

Ming Jin
Tongji University
95 PUBLICATIONS **1,907** CITATIONS
SEE PROFILE

Jean-Pierre Malval
Université de Haute-Alsace
74 PUBLICATIONS **632** CITATIONS
SEE PROFILE

CHEMISTRY OF MATERIALS

Article

pubs.acs.org/cm

Excited-State Dynamics of a D-π-A Type Sulfonium-Based Alkoxystilbene Photoacid Generator

Vincent De Waele,*[,⊥] Maximilian Hamm,[⊥] Thomas Vergote,[‡,§] Hélène Chaumeil,[§] Ming Jin,[†] Jean-Pierre Malval,[‡] Patrice Baldeck,[∥] and Olivier Poizat*[,⊥]

[⊥]Laboratoire de Spectrochimie Infrarouge et Raman, UMR CNRS 8516, Université de Lille1 - Sciences et Technologies, Cité Scientifique, 59655 Villeneuve d'Ascq Cedex, France

[‡]Institut de Sciences des Matériaux de Mulhouse, UMR 7361, Université de Haute-Alsace, 15 Rue Jean Starcky, 68057 Mulhouse, France

[§]Laboratoire de Chimie Organique et Bioorganique, EA4566, Université de Haute-Alsace, ENSCMu, Institut Jean-Baptiste Donnet, 3 bis rue A. Werner, 68093 Mulhouse, France

[†]Institute of Functional Polymer Materials, Tongji University, 1239 Siping Road, 200092 Shanghai, P. R. China

[∥]Laboratoire Interdisciplinaire de Physique, UMR CNRS 5588, Université Joseph Fourier, 38402 Saint Martin d'Hères, France

Supporting Information

ABSTRACT: The excited-state relaxation dynamics of a D-π-A sulfonium-based alkoxystilbene photoacid generator has been investigated in acetonitrile solution by using femtosecond transient absorption and nanosecond laser flash photolysis experiments. For the first time, the successive reaction steps involved in the photoinduced proton generation of a sulfonium acid generator have been kinetically and spectrally resolved from the early stages (femtosecond time scale) to the final chemical processes (microsecond domain). An overall four-step reaction scheme is established, and two main deactivation pathways limiting the proton generation efficiency are identified and quantified.

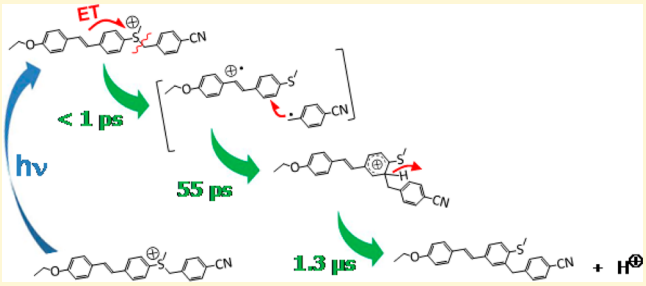

INTRODUCTION

Photoacid generators (PAGs) able to produce H^+ upon irradiation constitute an important class of cationic photoinitiators of polymerization widely used for industrial applications in the fields of photoresists,[1,2] microelectronics,[3] photosensitized resins,[4−6] and 3D-microfabrication.[6] In particular, sulfonium salts are often employed as photoacid generators in chemically amplified resists.[3,7−11] In order to limit the photodegradation, improve the spatial resolution, and open up the possibility of in-depth activation for applications such as 3D-lithography, the development of two-photon activable PAGs systems that can be excited with long-wavelength light has attracted much interest.[3,7,12−18] The basic principle is to associate a two-photon active sensitizer with a PAG. The acid generation generally proceeds through a photoinduced electron transfer (PET) from the excited photosensitizer to the PAG. A possible strategy is to mix two independent molecules, in which case photosensitization is a bimolecular process and occurs via an intermolecular PET with a kinetics limited by diffusion. An alternative approach consists in coupling in a single molecular system the two-photon absorption and acid generation functionalities, in which case acid generation is sensitized via an intramolecular PET. Such bifunctional molecules based on arylsulfonium salt photoinitiators exhibiting both a high quantum yield for acid generation (Φ_{H^+}) and a large two-photon absorption cross-section were first reported by Perry et al.[15,19,20] and Belfield et al.[21,22] More recently, our working group has extended these pioneering approaches with the design of several D-π-A sulfonium-based PAGs showing effective two-photon sensitivity in the NIR region,[23−25] in which electron donor 4-substituted stilbene derivatives are linked in the *para* or *meta* position to methyl-benzyl sulfonium groups.

Understanding in detail the mechanism of H^+ release upon photoactivation is an essential prerequisite for being able to design new PAGs with improved efficiency. The studies reported so far on the photochemistry of sensitizer-bound sulfonium salts[26−31] rely essentially on product analysis and laser flash photolysis measurements. A broadly accepted mechanism has been established,[28] which outlines the key steps of the process (Scheme 1). After $\pi\pi^*$ excitation of the attached aryl chromophore, through-space or through-bond intramolecular PET to a low-lying σ^* LUMO of the sulfonium moiety (*step A*) occurs in competition with fluorescence and

Received: December 5, 2014
Revised: February 12, 2015
Published: February 23, 2015

DOI: 10.1021/cm504474g
Chem. Mater. 2015, 27, 1684−1691

Scheme 1. Photoacid Generation Mechanism Proposed for Sensitizer-Bound Sulfonium PAGs[a]

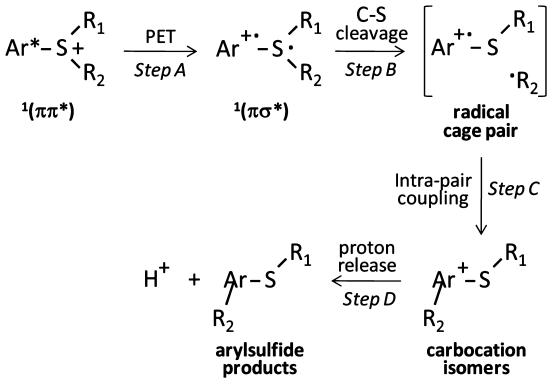

[a]From ref 28.

nonradiative deactivation. Subsequent homolytic cleavage of a sulfonium C−S bond (*step B*) produces a singlet radical/cation radical pair. The cleavage process being assumed to be faster than back ET, which takes place in the Marcus inverted region,[30] its efficiency is expected to be directly correlated to the quantum yield of the initial PET. In fact, the PET-induced bond cleavage can be a two-step process, as depicted in Scheme 1, or a concerted electron transfer and bond breaking process. The question has been investigated in detail by cyclic voltammetry for a series of arylsulfonium cations differing by the nature of the aryl chromophore and/or the leaving alkyl group R_2.[29] It is concluded that the higher the aryl π^* MO energy (driving force) and the weaker the C−S bond strength, the greater the tendency for the concerted mechanism to prevail over the stepwise mechanism. The radical pair then undergoes in-cage radical coupling (*step C*) to produce a distribution of transient carbocationic regioisomers corresponding to the possible sites of the arylsulfide cation radical able to accommodate radical $^{\bullet}R_2$. These are the aryl carbon sites possessing a proton, the release of which (*step D*) allows stabilizing the corresponding rearrangement products. The regioselectivity has been rationalized in terms of spin density of these carbon sites[26,28] and their distance with the radical $^{\bullet}R_2$ reactive carbon.[32] Finally deprotonation of the carbocation isomers in the presence of water yields stable neutral arylsulfide products (*step D*). This ultimate step of the photoacid generation chain process, characterized by laser flash photolysis, takes place in the microsecond time domain.[31,33,34]

In addition, it has been established that the overall photorearrangement efficiency is limited by the possible existence of several parallel relaxation processes of the radical cage pair competing with the in-cage radical coupling (*step C*):[26−28,32] radical cage escape by diffusion, reformation of the starting arylsulfonium cation by in-cage radical recombination without rearrangement, and, in acetonitrile solvent in the presence of trace water, intrapair electron transfer followed by reaction with solvent molecules to produce neutral sulfide and amide products, which also leads to proton release. Strong influence of solvent viscosity on the photoproducts distribution has been found to inform on the radical cage pair behavior.[32] Increasing the viscosity appears to decrease the efficiency of intrapair rearrangement in favor of reformation of the starting sulfonium salt, to increase the ratio of rearrangement products to escape products, and to inhibit the formation of the more distant rearranged products. These results indicate that, as expected, processes involving the largest-amplitude reorientation are the most viscosity-dependent.

Despite these studies, if the overall mechanism of photoinduced H^+ release given in Scheme 1 seems well-established, the short-time reaction dynamics remain practically not investigated. Time-resolved spectroscopic investigations have been mostly restricted to the microsecond time range, but the subnanosecond domain, where most of the key elementary reaction steps in Scheme 1 (*steps A-C*) are expected, has not been explored. The kinetics of PET induced bond cleavage and of intrapair radical coupling are unknown. Direct detection and characterization of the main short-lived chemical intermediates involved in the reaction are lacking.

In this respect, we have started an in-depth study of the photophysics and excited-state dynamics of some D-π-A sulfonium-based PAGs designed for two-photon absorption. We report here on an investigation by pump−probe time-resolved absorption spectroscopy of the photoreactivity in acetonitrile solution of a 4-ethoxystilbene derivative substituted in position 4′ by a methyl(*p*-cyanobenzyl)sulfonium (EtO-PS, see Scheme 2), which combines efficient two-photon

Scheme 2. Molecular Structure of Sulfonium EtO-PS and Its Precursor Sulfide ETMS

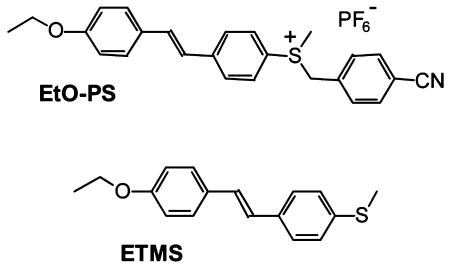

absorption and acid generation properties.[23] The main reaction steps leading to photoinduced proton release are identified and kinetically characterized from the early stages (femtosecond time scale) to the final chemical processes (microsecond domain). The 4-ethoxy-4′-thiomethyl-stilbene (ETMS, see Scheme 2), precursor sulfide of EtO-PS,[23] is also studied to help identify the transient cation radical product of EtO-PS cleavage and as a model compound able to mimic the photophysical behavior of the final arylsulfide photoproducts.

EXPERIMENTAL SECTION

The synthesis procedure and characterization of 4-ethoxy-4′-methyl(*p*-cyanobenzyl)sulfonium stilbene hexafluorophosphate (EtO-PS) and of its neutral precursor sulfide 4-methoxy-4′-thiomethyl-stilbene (ETMS) have been detailed elsewhere.[23] Acetonitrile (MeCN) solvent (spectroscopic grade purity) and 9,10-dicyanoanthracene (DCA, 97%) were provided by Sigma-Aldrich and used without further purification. UV−vis steady-state absorption measurements were done with a Cary100 spectrophotometer. Steady-state fluorescence measurements were performed on a Varian Cary Eclipses spectrometer. Emission spectra were spectrally corrected. The UV−visible spectroelectrochemistry setup, coupling a multichannel detection spectrophotometer to cyclic voltammetry (potential scan rate 0.002 V s^{-1}) and involving a spectroelectrochemical cell designed for working under *quasi* thin layer diffusion conditions (<100 μm), has also been precisely detailed previously.[35]

Nanosecond transient absorption experiments were carried out using a conventional laser flash photolysis apparatus. Excitation pulses at 350 and 425 nm (fwhm 8 ns, 1 mJ) were provided by a 10-Hz Nd:YAG laser (Continuum Surelite II) coupled to an OPO

DOI: 10.1021/cm504474g
Chem. Mater. 2015, 27, 1684−1691

(Continuum Panther EX OPO) and SH05 shutter (Thorlabs). The probe light was provided by a pulsed Xe lamp (XBO 150W/CR OFR, OSRAM). The transmitted light was dispersed by a monochromator (Horiba Jobin-Yvon, iHR320) and analyzed with a photomultiplier (R1477-06, Hamamatsu) coupled to a digital oscilloscope (LeCroy 454, 500 MHz). Synchronization of excitation pulses and acquisition time was secured with PCI-6602 8-Channel counter/timer (National Instruments). The experiment was controlled by homemade software written in LabView environment. Kinetic traces at each wavelength were averaged over 9 to 25 laser shots. The deconvolution of the individual kinetics with the experimentally measured instrument response function (IRF) leads to 10 ns time resolution. Spectra were reconstructed from all the kinetics. Samples were contained in a quartz cell (10 × 10 mm^2 section) at an adjusted concentration ($\sim 10^{-3}$ mol dm^{-3}) to get an absorption value of about 1.0 at the pump excitation wavelength. For measurements in deaerated conditions, sample solutions were treated by bubbling N_2 for 30 min.

The femtosecond transient absorption setup used in this study was already described in detail elsewhere.[36] Briefly, it involves a 1-kHz Ti:sapphire laser system (Coherent, BM Industries) which delivers 100 fs (0.8 mJ) pulses at 800 nm. Pump excitation at 325 or 350 nm was obtained by using a Quantronix femtosecond optical parametric amplifier (Palitra-FS-UV3) pumped at 800 nm. The pump pulse energy at the sample was about 2 μJ (0.2 mJ cm^{-2}). The white light continuum probe beam was generated by focusing the fundamental beam in a 1 mm CaF_2 rotating plate. The pump−probe polarization configuration was set at the magic angle (54.7°), and the probe pulse was delayed in time relative to the pump pulse using an optical delay line (Microcontrol Model MT160-250PP driven by an ITL09 controller, precision: 0.1 μm). The white light continuum was split into a probe beam collinear with the pump beam in the sample cell and a reference beam parallel to it and passing through the sample out of the pump beam. The transmitted probe and reference lights were dispersed with a spectrograph and detected on two different channels of a CCD optical multichannel analyzer (Princeton Instrument LN/CCD-1340/400-EB detector with ST-138 controller). Notch filters were placed between the sample cell and the detector to attenuate the pump-pulse related noise. Sample solutions ($\sim 10^{-3}$ mol dm^{-3}, OD = 1 at the pump wavelength) were circulated in a flow cell with 200 μm entrance window thickness and 2 mm optical path length. In this configuration, the instrumental response function at a given wavelength (IRF, full-width at half-maximum of the pump−probe intensity cross correlation) was estimated at about 130 fs from the two-photon (pump + probe) absorption signal in pure HEX and by measuring the stimulated Raman amplification signal from the solvent. The time dispersion of the continuum light, essentially due to its generation plate and the sample itself, was about 350 fs over the 350−700 nm region of analysis. Pump−probe absorption (PPA) spectra were accumulated over 3 min (~180000 pump−probe sequences). The characteristic times at any specific wavelength were obtained by fitting the corresponding kinetics with the result of a multiexponential function convolved with a 130 fs fwhm Gaussian pulse (which approximates the pump−probe correlation function). The Gaussian center (time-zero) was adjusted for each wavelength according to the continuum dispersion curve. More information about the experimental time-resolution and the fitting procedure are given in the Supporting Information.

It is important to note that, because the sulfonium bond-breaking process is an irreversible reaction, fast reagent consumption and accumulation of the arylsulfide rearrangement products occur upon photoexcitation. On the other hand, due to the reduced quantity of available EtO-PS, using quite large volumes of circulating sample solution was not realistically feasible. Great care was thus taken to limit the measuring time of each fresh sample below a tolerable irradiation threshold. To this end, sample degradation was checked by steady-state absorption after each experiment by reference to previous data describing the spectral evolution of EtO-PS under continuous irradiation.[23] Further evidence of the sample evolution could be obtained directly from the PPA spectra. Indeed, the arylsulfide photoproducts being themselves photoexcitable at 325 or 350 nm, their formation was easily identified by the appearance in the PPA spectra of a contribution due to their own photophysics superimposed to that related to the EtO-PS phototransformation. This was reflected by the presence of new spectral components, mainly a negative stimulated emission signal in the 350−450 nm region and a positive absorption band in the 450−700 nm region (lifetime ~100 ps), similar to the transient spectra observed on 325 nm excitation of sulfide ETMS (Figure S1, Supporting Information), characterizing the arylsulfide $S_1(\pi\pi^*)$ state. As a whole, by using for each experiment a 80 mL circulating solution and restricting the kinetic measurements to a maximum of 30 distinct pump−probe time delays, sample phototransformation was limited to a reasonable rate of 5−10%. Accordingly, group velocity dispersion (GVD) correction, which requires long series of measurements at numerous pump−probe time delays, could not be applied to the experimental transient spectra presented below.

RESULTS AND DISCUSSION

Femto-Picosecond Measurements. Subpicosecond pump−probe absorption (PPA) spectra of EtO-PS in MeCN have been recorded in the 0−1 ns time domain following pump excitation at 325 nm (Figure 1) and 350 nm (Figure S2, Supporting Information), i.e., on the high-energy side and in the vicinity of the band maximum, respectively, of the strong $\pi\pi^*$ transition of the stilbene chromophore (λ_{max} 347 nm[23]).

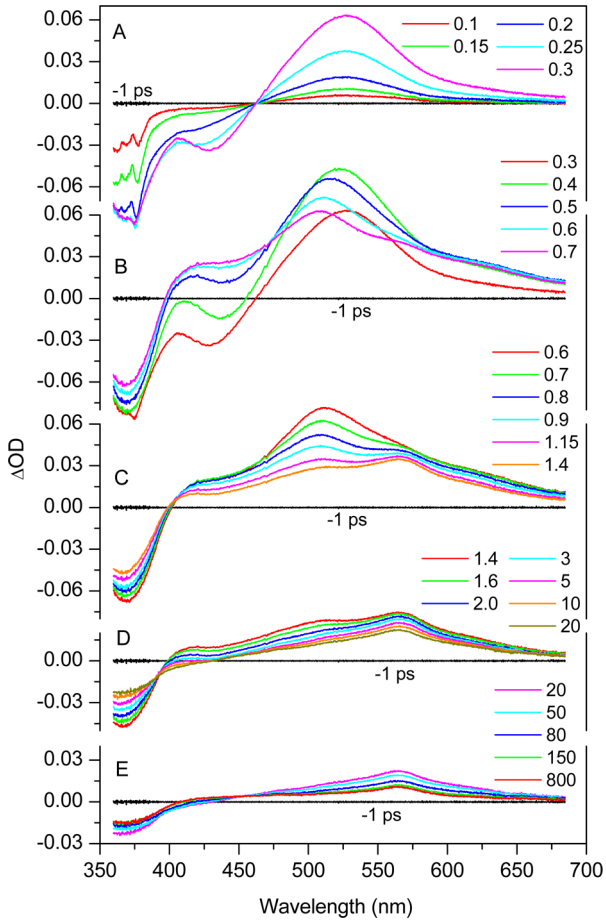

Figure 1. Typical PPA spectra of EtO-PS in MeCN recorded after pump excitation at 325 nm. For clarity, the spectral evolution is separated in 5 time domains 0−0.3 ps (A), 0.3−0.7 ps (B), 0.6−1.4 ps (C), 1.4−20 ps (D), and 20−800 ps (E). The time delays (ps) are indicated. The −1 ps trace corresponds to the spectral baseline in the absence of pump excitation.

DOI: 10.1021/cm504474g
Chem. Mater. 2015, 27, 1684−1691

Similar results were obtained in both cases, but, with the 325 nm excitation, the analyzed spectral window could be sufficiently extended in the UV region to clearly reveal the negative ground-state bleach signal (GSB). The femto-picosecond spectral evolution is rather complex due to the combined effects of multiple band shifts and changes in shape and intensity occurring in the same time window. In fact, photoinduced reaction steps A-C (Scheme 1), excited-state conformational changes, and vibrational cooling and solvation of the successive excited-state species and chemical intermediates, as well as of the ground-state molecules partly renewed from direct internal conversion, are more or less concomitant. The associated kinetics cannot be analyzed globally using a reasonably restricted sum of exponential functions. However, the 0−1 ns spectral evolution can be roughly divided into four main stages, in addition to the initial signal appearance related to the instrumental rise time, for which approximate time constants τ_1−τ_4 can be determined by averaging the values found from independent multiexponential fits of the kinetics performed at few distinct wavelengths within the various GSB, TA, and SE band positions. These average time constants are listed in Table 1. Typical kinetic plots are shown in Figures S3 and S4 of the Supporting Information together with the corresponding fits.

Table 1. Time Constants τ_1−τ_5 Determined for the Photoinduced Proton Generation Process in EtO-PS in MeCN

τ_1 (ps)	τ_2 (ps)	τ_3 (ps)	τ_4 (ps)	τ_5 (μs)
0.18 ± 0.04	0.37 ± 0.07	3.5 ± 0.5	55 ± 6	1.3 ± 0.1

In the subpicosecond range (Figure 1, part A), one observes first the rise of a spectrum characterized by a broad transient absorption (TA) band peaking at 528 nm and two negative bands at about 430 nm and below 400 nm, respectively. The latter one corresponds to the position of the ground-state absorption (Figure S5, Supporting Information) and is readily assigned to GSB. A fine band structure superimposed to the GSB band at time delays shorter than 0.4 ps is due to stimulated Raman scattering from both solute and solvent arising during the pump−probe overlap. The intensity of the Raman peaks follows the pump−probe cross-correlation, and thus their dynamics can be used for measuring the IRF. The 430 nm negative band cannot be ascribed to a GSB signal since EtO-PS does not show any ground-state absorption in this domain. It is likely due to stimulated emission (SE) as it corresponds to the region of the fluorescence spectrum (see Figure S5). The rising kinetics of all three bands are identical and properly taken into account by the IRF convolution procedure. Therefore, they characterize the IRF-limited appearance of the transient spectrum of the first populated stilbene-centered emissive excited singlet $\pi\pi^*$ state. The overall shape of this spectrum (0.3 ps trace in Figure 1) indeed resembles that reported for the $S_1(\pi\pi^*)$ state of stilbene[37] although notable red-shifts of the GSB (∼50 nm) and SE (∼80 nm) band position and larger Stokes shift (5560 cm^{-1} vs 3590 cm^{-1}) are observed for EtO-PS due to the push−pull character of the structure induced by the presence of electron donor and acceptor groups at *para* positions.

The $S_1(\pi\pi^*)$ spectrum evolves rapidly, the most impressive change being the total fading of the SE signal, which occurs with a single-exponential kinetics of time constant τ_1 = 0.18 ± 0.04 ps and is nearly completed at ∼0.7 ps (Figure 1, part B). Simultaneously a partial decrease in intensity of the TA band together with its blue shift by ca. 20 nm is observed (τ_{shift} = 0.16 ± 0.03 ps, see Supporting Information Figure S6). The extinction of the SE provides strong evidence that this first stage of the spectral evolution is due to the ultrafast depopulation of the emissive stilbene-centered $\pi\pi^*$ state. Stilbene compounds are known to undergo efficient excited S_1-state quenching by trans−cis photoisomerization; however, the 0.18 ps lifetime of the stilbene-centered $\pi\pi^*$ state in EtO-PS is drastically shorter than the S_1-state lifetime of stilbene (40 ps[37]) and the stilbene sulfide ETMS (122 ps, see Supporting Information Figure S1). It is consistent with the existence in the case of EtO-PS of a further ultrafast quenching process by intramolecular electron transfer to the sulfonium group (*step A* in Scheme 1). Therefore, the 0.7 ps spectrum (TA band λ_{max} = 508 nm) characterizes a transient species, named hereafter $W^{508\ nm}$, which is either the $\pi\sigma^*$ excited singlet state localized on the sulfonium moiety or, in the case of concerted PET-induced bond cleavage, the singlet radical/cation radical pair. This point will be clarified later in this paper. Note that, in the GSB kinetics, there is no decay component corresponding to time τ_1, which points to the absence of direct ground-state repopulation from the stilbene-centered $\pi\pi^*$ state and confirms that quenching via trans−cis isomerization does not compete significantly with intramolecular ET. We also observe in Figure 1 (traces A and B) that a notable dynamic red-shift of the SE band takes place, whereas it decays. It reflects the presence of some molecular relaxation occurring in the S_1 ($\pi\pi^*$) state in parallel with the depopulation of this state. The charge transfer character of the S_1 state and the time scale of this red-shift strongly suggest a solvation process (MeCN solvent relaxation dynamics $\langle\tau_s\rangle$ = 0.26 ps[38]) although some contribution from intramolecular vibrational relaxation cannot be excluded.

The subsequent spectral evolution in the subnanoscond time range shows the concomitant decay of part of the GSB and TA signals with approximately three main stages characterized by three distinct isosbestic points. In the former stage (∼0.7−1.4 ps time period, part C in Figure 1), the 508 nm TA band declines, whereas a new TA band maximizing at 565 nm appears. Roughly half of the GSB intensity disappears simultaneously (isosbestic point at 405 nm). These spectral changes are characterized by a common time constant τ_2 = 0.37 ± 0.07 ps over the whole spectral range. They clearly reflect the ultrafast decay of the $W^{508\ nm}$ species, which leads to partial ground-state repopulation in competition with the formation of a new transient species absorbing at 565 nm, hereinafter referred to as $X^{565\ nm}$. The nature of this transient species will be discussed further below.

In the next stage (∼1.4−20 ps time period, part D in Figure 1), the GSB keeps decaying, while the 565 nm TA band becomes narrower and decreases in intensity to some extent, with a global time constant τ_3 = 3.5 ± 0.5 ps (isosbestic point at 392 nm). This evolution is not readily identifiable. Note the presence in the 1.4 ps spectrum of an apparent TA component at ca. 420 nm, on the red edge of the GSB band, which progressively narrows and undergoes a continuous blue-shift; whereas it decays until 20 ps, at which time it has completely disappeared. Such spectral characteristics are reminiscent of a hot ground-state absorption (HotGSA) overlapped with the GSB band, i.e., absorption by ground-state molecules having an excess of vibrational energy. Therefore, we suggest that time τ_3 might correspond, a least in part, to the dynamics of vibrational

DOI: 10.1021/cm504474g
Chem. Mater. 2015, 27, 1684−1691

cooling of hot molecules arising from the ultrafast partial ground-state repopulation occurring in the preceding step (time τ_2). Accordingly, based on the overall intensity decrease observed for the GSB component at the end of the cooling dynamics (sum of the preexponentiel factors found at 365 nm for the GSB decay kinetics during the τ_2 and τ_3 dynamics), a total ground-state recovery of ~70% can be estimated to take place during the τ_2 dynamics. It can be concluded that ~30% of the $W^{508\ nm}$ population leads to the $X^{565\ nm}$ intermediate.

Finally, an ultimate subnanosecond evolution (~5−300 ps time domain, parts D and E in Figure 1) shows mainly the decay by about 75% of the 565 nm TA band intensity simultaneously with a slight decrease of the GSB, with a time constant of $\tau_4 = 55 \pm 6$ ps. After 300 ps, the spectrum does not evolve anymore up to 1500 ps. The decay of the 565 nm TA is accompanied by a significant spectral narrowing of the band, without modification of the peak position. This change in band shape reveals that the 55 ps dynamics is not simply reflecting a depopulation process but also some structural evolution. In other words, the long-lived transient species persisting after 300 ps, named $Y^{565\ nm}$, resembles somewhat the precursor species $X^{565\ nm}$ but still is not strictly similar. On the other hand, a novel isosbestic point is present at 452 nm due to the emergence of some positive signal in the 400−430 nm region, reflecting the rise of a weak TA band simultaneously with the decay of the 565 nm TA band. The presence of this band is clearly apparent in the differential spectrum obtained by subtracting the 80 ps spectrum from the 300 ps one (λ_{max} ~ 420 nm, see Supporting Information Figure S7). It reveals the appearance of a further transient species, named $Z^{420\ nm}$, produced simultaneously with $Y^{565\ nm}$ from $X^{565\ nm}$. Finally, the GSB intensity drops again by about 35%, stabilizing at 300 ps at ~20% of its initial value at 0.3 ps.

Nano-Microsecond Measurements. To complete these data, laser flash photolysis spectra of EtO-PS were recorded in aerated MeCN in the nano-microsecond time domain following pump excitation at 350 nm (Figure 2). The shorter-time spectrum (0.1 μs) very closely resembles the 300 ps spectrum in Figure 1. A main band peaking at 560 nm and decaying in tens of microseconds with second-order kinetics (Figure S8, Supporting Information) correlates nicely with the residual 565 nm TA band observed at 300 ps and thus corresponds to the $Y^{565\ nm}$ transient species. The kinetics becomes faster upon increasing the sample concentration, as expected for a diffusional bimolecular recombination process. In the blue region, a much faster decay kinetics, nearly completed at a time delay of 2 μs and well fitted to a single-exponential function of time-constant $\tau_5 = 1.3 \pm 0.1$ μs (Figure S8, Supporting Information), denotes the presence of another transient species. A similarly fast kinetics is noticed above 625 nm. Subtracting the 2 μs spectrum from the 0.1 μs one after normalization with respect to the 560 nm peak intensity reveals the spectral signature of the fast decaying species (Figure 2, part B). As expected, it displays a blue absorption band with λ_{max} at 400−420 nm that matches quite well the weak TA band rising in the 20−300 ps time range and ascribed above to the $Z^{420\ nm}$ species (see the [300 ps −80 ps] differential spectrum in Supporting Information Figure S7). It also shows a weaker broad and nearly flat absorption in the 500−700 nm domain.

Both the first-order kinetics in the blue and red regions and second-order kinetics at 560 nm appear insensitive to sample deaeration by bubbling N_2, which indicates that neither the $Z^{420\ nm}$ nor the $Y^{565\ nm}$ transient species present at 300 ps and

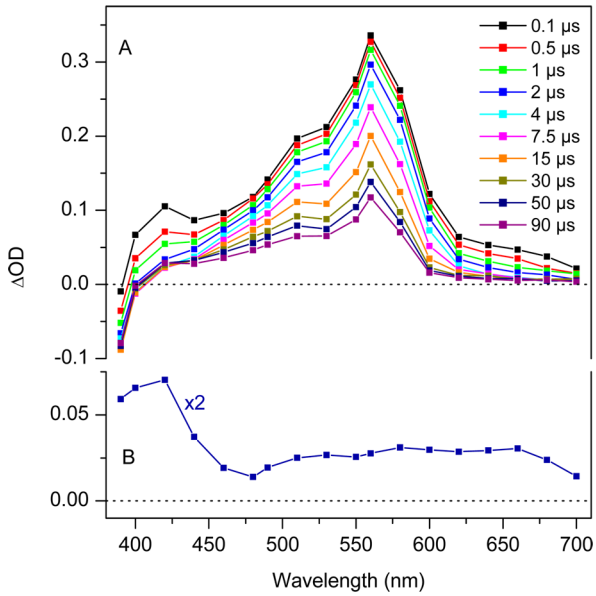

Figure 2. Laser flash photolysis spectra obtained at different time delays from 100 ns to 90 μs after excitation at 350 nm of EtO-PS in MeCN (A) and differential transient spectrum obtained by subtracting the 2 μs spectrum from the 0.1 μs one after normalization with respect to the 560 nm peak intensity (B).

decaying in the microsecond time domain are assignable to an excited triplet state. It is worthy of note that, whereas the 560 nm kinetics also remains unchanged upon addition of water in the solution, the first-order kinetics appears strongly shortened in the presence of water (see Figure S8, Supporting Information).

Spectral Characterization of the $ETMS^{\bullet+}$ Cation Radical. Until now, only the shortest-time transient spectrum observed following photoexcitation of EtO-PS has been firmly identified and ascribed to an initially populated excited S_1 ($\pi\pi^*$) state localized on the stilbene chromophore. The subsequent spectra arising in the picosecond to microsecond time range remain to be assigned. In that perspective, a key issue is the spectral identification of the arylsulfide cation radical produced from the homolytic cleavage process, which corresponds to the oxidized form of the ETMS molecule, $ETMS^{\bullet+}$. First attempts to detect the transient $ETMS^{\bullet+}$ species independently by UV−visible spectroelectrochemistry under *quasi* thin layer diffusion conditions (cyclic voltammetry technique) failed because this cation radical is too short-lived to allow a substantial stationary concentration to take place at the electrode surface. $ETMS^{\bullet+}$ was thus generated by photosensitized oxidation in air-saturated MeCN using 9,10-dicyanoanthracene (DCA) as sensitizer, according to a procedure similar to that reported for stilbene compounds.[39,40] Photo-oxidation of ETMS by the S_1 state of DCA was achieved upon pulse excitation at 425 nm, and the absorption spectra were obtained by laser flash photolysis. In the absence of DCA, no transient spectrum is observed because ETMS alone does not absorb at 425 nm. In the presence of DCA (Figure 3, trace A), a strong transient absorption band peaking at 560−570 nm and decaying via second-order kinetics in the microsecond time domain, not observed for pure DCA solution, is readily assigned to photosensitized $ETMS^{\bullet+}$. The broad absorption of the anion radical $DCA^{\bullet-}$ in the 650−750 nm region[41] is not observed as it is quenched by oxygen.[39,40]

DOI: 10.1021/cm504474g
Chem. Mater. 2015, 27, 1684−1691

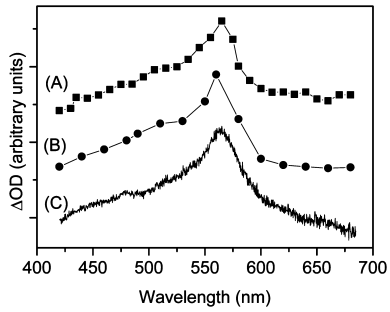

Figure 3. Comparison of the (A) flash photolysis spectrum of ETMS cation radical produced by photosensibilized oxidation in the presence of DCA, (B) 90 μs flash photolysis spectrum of EtO-PS (from Figure 2), and (C) 300 ps PPA spectrum of EtO-PS (from Figure 1). The solvent is MeCN in all cases.

Overall Excited-State Dynamics. We present below a meticulous analysis of the above spectrokinetic data that leads to a global picture of the excited-state relaxation dynamics governing the property of photoacid generation of EtO-PS in MeCN solvent (reaction scheme in Figure 4). As seen in Figure 3, the reference spectrum of photosensitized ETMS$^{\bullet+}$ (trace A) is undeniably similar, in band position and band shape, to the 300 ps PPA spectrum recorded after photoexcitation of EtO-PS (trace C) or the flash photolysis spectrum observed in the microsecond domain (trace B). We conclude that, in the spectrokinetic evolution of EtO-PS, the TA band observed at ca. 565 nm at 300 ps and decaying with second-order kinetics in tens of microseconds ($Y^{565\ nm}$ species) characterizes the free, solvated cation radical resulting from radical cage escape after photocleavage of the molecule. Note that the other species expected to be produced in the cleavage of EtO-PS, the *p*-cyanobenzyl radical, cannot be detected in our measurements as it does not absorb above 330 nm.[42,43] On this basis, starting from the 300 ps PPA spectrum in Figure 1 and going back in time allows for a step-by-step identification of the short-time reaction dynamics.

The preceding 20−300 ps spectral evolution (time τ_4), marked by the progressive narrowing and 75% decrease in intensity of the 565 nm band, is likely assigned to the dynamics of cage escape competing with in-cage radical coupling. The $X^{565\ nm}$ species is thus identified as the in-cage cation radical ETMS$^{\bullet+}$. A broader absorption band shape for the in-cage cation radical compared to the free species can be explained by an incomplete solvation and by the possible existence of some structural disorder due to a distribution of radical/cation radical mutual orientations within the pair. The decay by 75% of the 565 nm band on going from the in-cage to the free solvated species indicates that only one-quarter of the ETMS$^{\bullet+}$ cation radical and *p*-cyanobenzyl radical species produced from homolytic cleavage of EtO-PS escape the cage ($k_{esc} \sim 4.5 \times 10^9\ s^{-1}$), the three other quarters undergoing in-cage recombination (step *C* in Scheme 1). However, on the other hand, the fact that the GSB signal is reduced by ~35% in the same time means that one-third of the in-cage radical species recombine with no rearrangement, reforming the starting arylsulfonium cation ($k_{CnR} \sim 6.4 \times 10^9\ s^{-1}$). Therefore only ca. 40% of the in-cage radicals undergo in-cage recombination with rearrangement to produce acidic carbocations ($k_{CR} \sim 7.3 \times 10^9\ s^{-1}$). We thus propose that the weak TA band appearing simultaneously in the 400−430 nm region ($Z^{420\ nm}$ species, 300 ps−80 ps differential spectrum in Supporting Information Figure S7) and decreasing in the microsecond time range with lifetime τ_5 (Figure 2) corresponds to carbocationic species resulting from this in-cage radical coupling with rearrangement. In this regard, the τ_5 dynamics can be related to the deprotonation process ultimately responsible for the acid generation property (*step D* in Scheme 1), which indeed has already been reported to occur in the microsecond time domain.[31,33,34] The notable shortening of τ_5 in the presence of water supports this assignment. Indeed, the released proton is

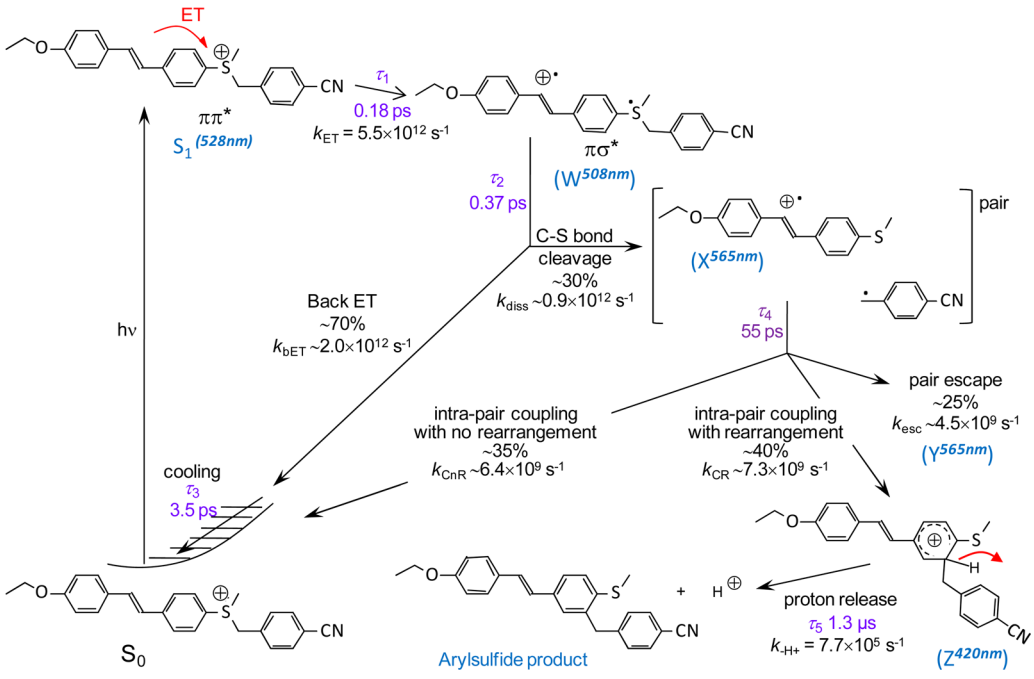

Figure 4. Overall photoacid generation mechanism and dynamics determined for EtO-PS in MeCN from the time-resolved absorption data. For clarity, only one of the possible carbocation regioisomers resulting from intrapair radical coupling has been represented.

DOI: 10.1021/cm504474g
Chem. Mater. 2015, 27, 1684−1691

expected to be stabilized by hydration in aqueous solution, thus speeding up the deprotonation reaction. For the same reason, the broad absorption band evidenced by laser flash photolysis in the 500−700 nm domain (Figure 2, part B) and showing the same kinetic behavior as the 400−430 nm band can also be ascribed to carbocationic product(s) of in-cage radical coupling.

At shorter time delays, two kinetic steps remain unassigned. One corresponds to the decay of the initially populated emissive S_1 ($\pi\pi^*$) state and the appearance of a nonemissive species $W^{508\ nm}$ (time τ_1). The second one (time τ_2) corresponds to the decay of $W^{508\ nm}$ and rise of the $X^{565\ nm}$ species that has just been identified as the in-cage $ETMS^{\bullet+}$ cation radical. Therefore, the τ_2 dynamics is likely characterizing the ultrafast sulfonium C−S bond homolytic cleavage (*step B* in Scheme 1). The precursor species $W^{508\ nm}$ (0.7 ps spectrum in Figure 1) is thus assigned with some confidence to the dark $\pi\sigma^*$ excited singlet state localized on the sulfonium moiety. However, it was noted ahead that part of the starting ground-state sulfonium is repopulated simultaneously with this reaction step. This observation reveals that intramolecular back electron transfer leads to efficient quenching of the $\pi\sigma^*$ excited state (∼70%, $k_{bET} \sim 2.0 \times 10^{12}\ s^{-1}$) in competition with the cleavage process (∼30%, $k_{diss} \sim 0.9 \times 10^{12}\ s^{-1}$). Back electron transfer was already suggested to be the major source of photocleavage inefficiency in the case of anthracene-sensitized photolyze of triphenylsulfonium salt in solution.[44] Finally, the τ_1 dynamics can be indisputably associated with the $^1\pi\pi^* \rightarrow {}^1\pi\sigma^*$ transition by excited-state intramolecular electron transfer from the stilbene moiety to the sulfonium group (step A in Scheme 1). Though the 508 nm absorption of the dark $\pi\sigma^*$ state (0.7 ps spectrum) is not strongly differentiated from the 528 nm absorption of the preceding emissive $\pi\pi^*$ state (0.3 ps spectrum), the decay kinetics of the $\pi\sigma^*$ state TA band at 508 nm is clearly delayed relative to the decay of the SE signal associated with the $\pi\pi^*$ state. In other words, the formation of the cation radical takes place after a short but detectable time delay following the $\pi\pi^*$ state depopulation. This delay shows explicitly that the intramolecular ET process involved in the $\pi\pi^*$ to $\pi\sigma^*$ transition (*step A*) and the C−S bond cleavage leading to the radical/cation radical pair (*step B*) are indeed two distinct subpicosecond reaction steps. The PET-induced bond cleavage in EtO-PS is thus a two-step process.

From the cumulated amount of ground-state repopulation occurring at the different stages of the reaction scheme (∼80%) estimated from the recovery of the GSB signal, on one hand, and the amount of excited molecules deactivated in the cage escape process (∼8%), on the other hand, the overall efficiency of the proton release process can thus be roughly evaluated to ∼12%. This value is somewhat uncertain as it is based on the approximation that the negative signal intensity measured at the position of the GSB component is indeed purely due to GSB, i.e., it is not affected, at any time, by the presence of superimposed TA bands interfering with the GSB signal. However, despite this rather crude approximation, the 12% value is in agreement with the quantum yield for acid generation measured previously ($\Phi_{H^+} = 0.1$).[23]

CONCLUSIONS

The photoinduced dynamics of a 4-ethoxystilbene derivative substituted in position 4′ by a methyl(*p*-cyanobenzyl)sulfonium (EtO-PS) showing photoacid generation properties has been investigated in acetonitrile solution by pump−probe time-resolved absorption spectroscopy. The main reaction steps leading to photoinduced proton release are identified and kinetically characterized from the early stages (femtosecond time scale) to the final chemical processes (microsecond domain). Direct population at $\lambda_{exc} > 300$ nm of the stilbene localized $\pi\pi^*$ singlet excited state is followed by a subpicosecond two-step PET-induced C−S bond homolytic cleavage yielding a radical/cation radical cage pair. The dissociation reaction occurs in a low-lying $\pi\sigma^*$ state of the sulfonium group populated by intramolecular ET from the initial $\pi\pi^*$ state. The stilbene sulfide cation radical product of cleavage has been clearly identified by its spectral signature previously characterized from the direct generation of this cation radical by photosensitized oxidation of the corresponding neutral sulfide molecule. In-cage radical coupling leads to acidic carbocationic adduct species with an average rate constant of $7.3 \times 10^9\ s^{-1}$. Finally, the carbocation species evolve by proton release in a few microseconds time range. This four-stage reaction dynamics nicely supports the broadly accepted mechanism proposed for sensitizer-bound sulfonium salts.[28] The proton generation efficiency is found to be limited mainly at two stages of the reaction scheme: (1) ultrafast back electron transfer quenches the $\pi\sigma^*$ excited state and limits the C−S bond homolytic cleavage efficiency to about 30%; then (2), at the stage of the radical cage pair, radical pair escape and in-cage radical coupling reforming the starting ground-state sulfonium both compete with in-cage radical coupling with rearrangement, finally reducing the efficiency of formation of acidic carbocation species to approximately 12%, a value in agreement with the quantum yield for acid generation measured previously ($\Phi_{H^+} = 0.1$).[23]

Further interesting issues for the future are to assess to what extent it is possible to control the photoinduced dynamics in view of increasing the overall yield of proton release Φ_{H^+} by modifying the environment properties or the arylsulfonium structure. In this connection, complementary investigations are currently developed to examine the influence of the solvent on the excited-state dynamics of EtO-PS and, in particular, find out which reaction steps are more specifically sensitive to the surrounding polarity and viscosity. On the other hand, comparative studies of the reaction dynamics of other D-π-A sulfonium-based alkoxystilbene differing by the substitution site of the (*p*-cyanobenzyl)sulfonium group are undertaken and will be reported shortly. An important objective will be to understand the previous observation of a strong enhancement of Φ_{H^+} through a *para*-to-*meta* positioning effect of the sulfonium substituent.[23,24]

ASSOCIATED CONTENT

Supporting Information

Complementary experimental details about the time-resolution and kinetic analysis procedure for the femtosecond transient absorption data and Figures S1−S8. This material is available free of charge via the Internet at http://pubs.acs.org.

AUTHOR INFORMATION

Corresponding Authors

*E-mail: vincent.dewaele@univ-lille1.fr (V.D.W.).
*E-mail: olivier.poizat@univ-lille1.fr (O.P.).

Notes

The authors declare no competing financial interest.

DOI: 10.1021/cm504474g
Chem. Mater. 2015, 27, 1684−1691

■ ACKNOWLEDGMENTS

Support from the Agence Nationale de la Recherche "Projet Blanc: 2PAGmicrofab (ANR-BLAN-0815-03)" is gratefully acknowledged.

■ REFERENCES

(1) Reichmanis, E.; Thimpson, L. F. In *Polymers in Microlithography: Materials and Processes (ACS. Symp. Ser. Vol. 412)*; Reichmanis, E., MacDonald, S. A., Iwayanagi, T., Eds.; American Chemical Society: Washington, DC, 1989; pp 1−24.
(2) Reichmanis, E.; Houlihan, F. M.; Nalamasu, O.; Neeman, T. X. In *Polymers for Microelectronics: Resists and Dielectrics (ACS. Symp. Ser. Vol. 537)*; Thompson, L. F., Willson, C. G., Tagawa, S., Eds.; American Chemical Society: Washington, DC, 1993; pp 2−24.
(3) Shirai, M.; Tsunooka, M. *Prog. Polym. Sci.* **1996**, *21*, 1−45.
(4) Billone, P. S.; Park, J. M.; Blackwell, J. M.; Bristol, R.; Scaiano, J. C. *Chem. Mater.* **2010**, *22*, 15−17.
(5) Barker, I. A.; Dove, A. P. *Chem. Commun.* **2013**, *49*, 1205−1207.
(6) Lee, K.-S.; Kim, R. H.; Yang, D.-Y; Park, S. H. *Prog. Polym. Sci.* **2008**, *33*, 631−681.
(7) Sun, H.-B.; Kawata, S. In *Advances in Polymer Science*; Springer-Verlag: Berlin, 2004; Vol. *170*; p 169.
(8) Zhou, W.; Kuebler, S. M.; Carrig, D.; Perry, J. W.; Marder, S. R. *J. Am. Chem. Soc.* **2002**, *124*, 1897−1901.
(9) Crivello, J. V.; Lam, J. H. W. *Adv. Polym. Sci.* **1984**, *62*, 1−48.
(10) Crivello, J. V. *J. Polym. Sci.: Polym. Chem. Ed.* **1996**, *34*, 3231−3253.
(11) Pappas, S. P. In *UV Curing: Science and Technology*; Pappas, S. P., Ed.; Technology Marketing Corporation: CT, 1985; Vol. *2*, pp 1−25.
(12) Kawata, S.; Sun, H.-B.; Tanaka, T.; Takada, K. *Nature* **2001**, *412*, 697−698.
(13) Kawata, S.; Sun, H.-B. *Appl. Surf. Sci.* **2003**, *208*−*209*, 153−158.
(14) Cumpston, B. H.; Ananthavel, S. P.; Barlow, S.; Dyer, D. L.; Ehrlich, J. E.; Erskine, L. L.; Heika, A. A.; Lee, I.-Y. S.; McCord-Maughon, D.; Qin, J.; Röckel, H.; Rumi, M.; Wu, X.-L.; Marder, S. R.; Perry, J. W. *Nature* **1999**, *398*, 51−54.
(15) Zhou, W.; Kuebler, S. M.; Yu, T.; Cammack, J. K.; Ober, C. K.; Perry, J. W.; Marder, S. R. *Science* **2002**, *296*, 1106−1109.
(16) LaFratta, C. N.; Fourkas, J. T.; Baldacchini, T.; Farrer, R. A. *Angew. Chem., Int. Ed.* **2007**, *46*, 6238−6258.
(17) He, G. S.; Tan, L. S.; Zheng, Q.; Prasad, P. N. *Chem. Rev.* **2008**, *18*, 1245−1330.
(18) Jin, M.; Malval, J.-P.; Versace, D.; Morlet-Savary, F.; Chaumeil, H.; Defoin, A.; Allonas, X.; Fouassier, J. P. *Chem. Commun.* **2008**, 6540−6542.
(19) Kuebler, S. M.; Braun, K. L.; Zhou, W.; Cammack, J. K.; Yu, T.; Ober, C. K.; Marder, S. R.; Perry, J. W. *J. Photochem. Photobiol., A* **2003**, *158*, 163−170.
(20) Yu, T.; Ober, C. K.; Kuebler, S. M.; Zhou, W.; Marder, S. R.; Perry, J. W. *Adv. Mater.* **2003**, *15*, 517−521.
(21) Yanez, C. O.; Andrade, C. D.; Belfield, K. D. *Chem. Commun.* **2009**, 827−829.
(22) Yanez, C. O.; Andrade, C. D.; Yao, S.; Luchita, G.; Bondar, M. V.; Belfield, K. D. *ACS Appl. Mater. Interfaces* **2009**, *1*, 2219−2229.
(23) Xia, R.; Malval, J.-P.; Jin, M.; Spangenberg, A.; Wan, D.; Pu, H.; Morlet-Savary, F.; Chaumeil, H.; Baldeck, P.; Poizat, O.; Soppera, O. *Chem. Mater.* **2012**, *24*, 237−244.
(24) Jin, M.; Xu, H.; Hong, H.; Malval, J.-P.; Zhang, Y.; Ren, A.; Wan, D.; Pu, H. *Chem. Commun.* **2013**, *49*, 8480−8482.
(25) Jin, M.; Hong, H.; Xie, J.; Malval, J.-P.; Spangenberg, A.; Soppera, O.; Wan, D.; Pu, H.; Versace, D.-L.; Leclerc, T.; Baldeck, P.; Poizat, O.; Knopf, S. *Polym. Chem.* **2014**, *5*, 4747−4755.
(26) Saeva, F. D.; Breslin, D. T. *J. Org. Chem.* **1989**, *54*, 712−714.
(27) Saeva, F. D.; Breslin, D. T.; Martic, P. A. *J. Am. Chem. Soc.* **1989**, *111*, 1328−1330.
(28) Saeva, F. D.; Breslin, D. T.; Luss, H. R. *J. Am. Chem. Soc.* **1991**, *113*, 5333−5337.
(29) Andrieux, C. P.; Robert, M.; Saeva, F. D.; Savéant, J.-M. *J. Am. Chem. Soc.* **1994**, *116*, 7864−7871.
(30) Saeva, F. D.; Garcia, E.; Martic, P. A. *J. Photochem. Photobiol., A* **1995**, *86*, 149−154.
(31) Pappas, S. P.; Tilley, M. G.; Pappas, B. C. *J. Photochem. Photobiol., A* **2003**, *159*, 161−171.
(32) Dektar, J. L.; Hacker, N. P. *J. Am. Chem. Soc.* **1990**, *112*, 6004−6015.
(33) Iu, K.-K.; Kuczynski, J.; Fuerniss, S. J.; Thomas, J. *J. Am. Chem. Soc.* **1992**, *114*, 4871−4878.
(34) Welsh, K. M.; Dektar, J. L.; Garcia-Garibaya, M. A.; Hacker, N. P.; Turro, N. J. *J. Org. Chem.* **1992**, *57*, 4179−4184.
(35) Gaillard, F.; Levillain, E. *J. Electroanal. Chem.* **1995**, *398*, 77−87.
(36) Buntinx, G.; Naskrecki, R.; Poizat, O. *J. Phys. Chem.* **1996**, *100*, 19380−19388.
(37) Kovalenko, S. A.; Dobryakov, A. L.; Ioffe, I.; Ernsting, N. P. *Chem. Phys. Lett.* **2010**, *493*, 255−258.
(38) Horng, M. L.; Gardecki, J. A.; Papazyan, A.; Maroncelli, M. *J. Phys. Chem. A* **1995**, *99*, 17311−17337.
(39) Spada, L. T.; Foote, C. S. *J. Am. Chem. Soc.* **1980**, *102*, 391−393.
(40) Lewis, F. D.; Bedell, A. M.; Dykstra, R. E.; Elbert, J. E.; Gould, I. R.; Farid, S. *J. Am. Chem. Soc.* **1990**, *112*, 8055−8064.
(41) Nakamura, M.; Miki, M.; Majima, T. *J. Chem. Soc., Perkin Trans. 2* **2000**, 1447−1452.
(42) Neta, P.; Behar, D. *J. Am. Chem. Soc.* **1981**, *103*, 103−106.
(43) Tokumura, K.; Nosaka, H.; Ozaki, T. *Chem. Phys. Lett.* **1990**, *169*, 321−325.
(44) DeVoe, R. J.; Sahyun, M. R.; Schmidt, E.; Serpone, N.; Sharm, D. K. *Can. J. Chem.* **1988**, *66*, 319−324.

DOI: 10.1021/cm504474g
Chem. Mater. 2015, 27, 1684−1691